THE JOURNAL OF PHYSICAL CHEMISTRY B

Article

pubs.acs.org/JPCB

Spectroscopic Investigation of the Carotenoid Deoxyperidinin: Direct Observation of the Forbidden $S_0 \rightarrow S_1$ Transition

Jordan A. Greco,[†] Amy M. LaFountain,[†] Naoto Kinashi,[‡] Tetsuro Shinada,[‡] Kazuhiko Sakaguchi,[‡] Shigeo Katsumura,[‡] Nikki Cecil M. Magdaong,[§] Dariusz M. Niedzwiedzki,[∥] Robert R. Birge,[†] and Harry A. Frank*[,†]

[†]Department of Chemistry, University of Connecticut, 55 North Eagleville Road, Storrs, Connecticut 06269-3060, United States

[‡]Graduate School of Science, Osaka City University, 3-3-138 Sugimoto, Sumiyoshi-ku, Osaka 558-8585, Japan

[§]Department of Biology, Washington University in Saint Louis, One Brookings Drive, St. Louis, Missouri 63130, United States

[∥]Photosynthetic Antenna Research Center, Washington University in Saint Louis, One Brookings Drive, St. Louis, Missouri 63130, United States

ABSTRACT: This paper presents a spectroscopic investigation of deoxyperidinin, a synthetic peridinin analogue in which the carbonyl functional group in peridinin was replaced by a nonconjugated methylene group. Steady-state and ultrafast time-resolved absorption and fluorescence spectroscopic experiments are carried out on deoxyperidinin in *n*-hexane and acetonitrile at room temperature and in 2-methyltetrahydrofuran at 77 K. The spectra of deoxyperidinin have higher vibronic resolution compared to those of peridinin. The higher resolution is due to a substantial reduction in both molecular conformational disorder and inhomogeneous broadening of the spectra of deoxyperidinin compared to peridinin. Features in the steady-state absorption spectrum of deoxyperidinin that are not evident in the spectrum of peridinin are unambiguously assigned to the forbidden S_0 $(1^1A_g^-) \rightarrow S_1$ $(2^1A_g^-)$ absorption transition. The characteristics of both the steady-state and time-resolved spectra are interpreted using EOM-CCSD, SAC-CI, and MNDO-PSDCI quantum computational formalisms that provided a theoretical framework for understanding the photophysical properties of the molecules.

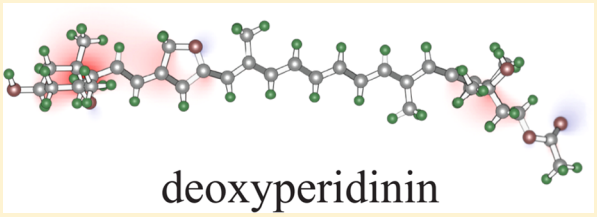

INTRODUCTION

Nature imposes restrictions in the form of quantum mechanical selection rules that determine which electronic states can undergo spectroscopic transitions by light absorption or emission. This is exemplified by the low-lying electronic states of polyenes and carotenoids for which a one-photon transition between the ground state with A_g^- symmetry and the first excited state, which has the same symmetry or pseudoparity, is forbidden.[1−4] However, a one-photon transition between the ground state and the second excited state, which has B_u^+ symmetry, is allowed.[5,6] Adherence to these selection rules may be relaxed by molecular distortions, configurational isomerization, functional group substitutions, or any other factors that reduce the symmetry of the molecule.[7] States for which radiative transitions are forbidden may also "borrow intensity" from neighboring "allowed" states via Herzberg−Teller coupling.[8] This interaction mixes states of different symmetry through vibronic motions and explains, for example, why polyenes and carotenoids exhibit S_1 $(2^1A_g^-) \rightarrow S_0$ $(1^1A_g^-)$ fluorescence and why the S_1 $(2^1A_g^-)$ emission is polarized in the same direction as fluorescence from the S_2 $(1^1B_u^+)$ state.[2] Allowedness of the radiative S_1 $(2^1A_g^-) \rightarrow S_0$ $(1^1A_g^-)$ transition is achieved by intensity borrowing from the S_2 $(1^1B_u^+)$ state. However, the emission from both the S_1 $(2^1A_g^-)$ and S_2 $(1^1B_u^+)$ states of polyenes and carotenoids is very weak and has quantum yields typically ranging between 10^{-3} and 10^{-6}.[9,10] Fortunately, the high sensitivity of photomultipliers on modern day emission spectrometers facilitates the detection of faint emission from these molecules, and many investigators have reported fluorescence from the low-lying "forbidden" S_1 $(2^1A_g^-)$ states of the biologically important, naturally occurring carotenoids and their parent polyenes.[10−16] The data have been used to deduce the energies of the S_1 $(2^1A_g^-)$ excited states and also to elucidate the mechanisms by which carotenoids transfer energy to (bacterio)chlorophyll in several pigment−protein complexes from photosynthetic organisms.[17,18]

An electronic transition from the S_0 $(1^1A_g^-)$ ground state to the S_2 $(1^1B_u^+)$ state is strongly allowed, has a very high oscillator strength, and is associated with the bright coloration of carotenoids in Nature.[7] In contrast, accessing the S_1 $(2^1A_g^-)$ state via direct absorption from the ground state is highly problematic. The exceedingly small S_0 $(1^1A_g^-) \rightarrow S_1$ $(2^1A_g^-)$ transition dipole and low oscillator strength make the direct detection of this transition via absorption spectroscopy very difficult.[19] Compounding the problem is that the transition is predicted to occur in the region where the long wavelength tail

Received: January 14, 2016
Revised: February 22, 2016
Published: February 23, 2016

DOI: 10.1021/acs.jpcb.6b00439
J. Phys. Chem. B 2016, 120, 2731−2744

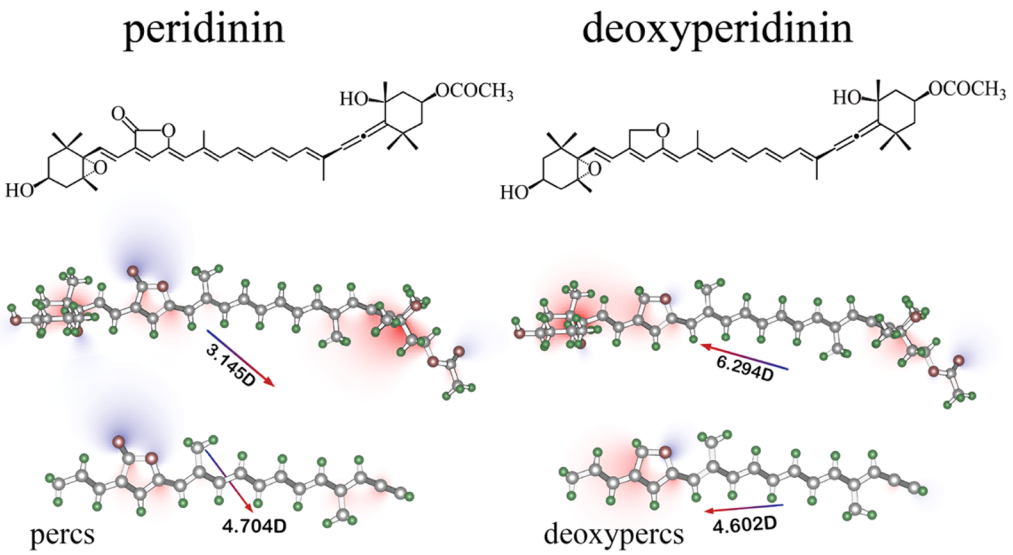

Figure 1. Structures of peridinin and deoxyperidinin. The molecular structures shown in the middle are for the full chromophores. The molecular structures shown at the bottom are simplified structures with C_s symmetry and are denoted percs (simplified peridinin) and deoxypercs (simplified deoxyperidinin). These model chromophores are used in most of the calculations reported in this paper. The intensity of the background color is proportional to the charge density, with excess positive charge shown in red and excess negative charge shown in blue. Dipole moment directions are shown with an arrow of arbitrary length where the tip of the arrow is positive and the label provides the magnitude in Debyes.

of the strongly allowed S_0 ($1^1A_g^-$) → S_2 ($1^1B_u^+$) absorption occurs, and this band can then overwhelm any absorption features associated with the S_0 ($1^1A_g^-$) → S_1 ($2^1A_g^-$) transition. Being able to detect the S_1 ($2^1A_g^-$) state via direct absorption would be very useful in understanding the precise molecular factors controlling light absorption and emission from these molecules, as well as the mechanism by which energy transfer from carotenoids to (bacterio)chlorophylls occurs. This is one of the most important functions of carotenoids in Nature.

Peridinin (Figure 1) is a prime example of a prolific light-harvesting carotenoid. It occurs naturally in many dino-flagellates and absorbs light in a region of the visible spectrum where chlorophyll (Chl) *a* is not a very efficient absorber.[20] It then transfers the absorbed energy with over 90% efficiency to Chl *a* for subsequent use in photosynthesis.[21−23] As can be seen in Figure 1, peridinin is a highly substituted molecule containing a lactone moiety and several other functional groups that reduce the overall symmetry of the π-electron conjugated system to a point where one might wonder whether symmetry-imposed selection rules apply at all to this molecule. Indeed, fluorescence originating from the S_1 ($2^1A_g^-$) state of peridinin is readily observed (Figure 2 in a number of solvents)[24−30] and a band proposed to be attributed to the very weak S_0 ($1^1A_g^-$) → S_1 ($2^1A_g^-$) absorption has been reported.[27] However, the presence of the carbonyl group in the lactone ring in peridinin gives rise to a large distribution of twisted conformations of the molecule in solution, broadening the line shape substantially and making weak absorption features especially difficult to discern. This effect is particularly evident in polar solvents (Figure 2).[26,30]

In the present work, deoxyperidinin, a peridinin analogue in which the carbonyl functional group has been replaced by a nonconjugated methylene group, was synthesized. Due to the absence of the carbonyl group, the spectral features of deoxyperidinin are narrower than those of peridinin owing to a substantial reduction in the distribution of conformers in solution. Moreover, in experiments carried out at 77 K, features in the steady-state absorption spectrum of deoxyperidinin can

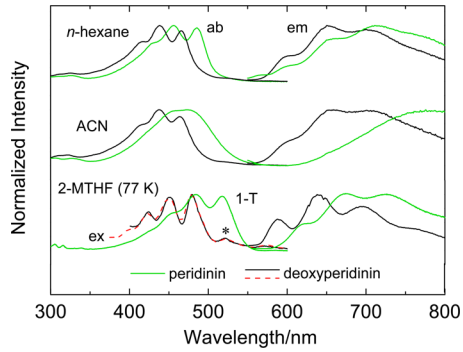

Figure 2. Absorption (ab) and fluorescence (em) spectra of peridinin and deoxyperidinin recorded in *n*-hexane and acetonitrile (ACN) at room temperature and in 2-MTHF at 77 K. The fluorescence spectra from deoxyperidinin were measured using an excitation wavelength of 464 nm in *n*-hexane and ACN, whereas those of peridinin were excited at 486 nm in *n*-hexane and 472 nm in ACN. The absorption spectra of the two molecules recorded in 2-MTHF at 77 K were converted to 1 − *T* for comparison and for the purpose of overlaying with the fluorescence excitation (ex) spectrum (red dotted trace) of deoxyperidinin which was detected at 689 nm. The asterisk indicates the spectral bands associated with the S_0 ($1^1A_g^-$) → S_1 ($2^1A_g^-$) absorption of deoxyperidinin.

be unambiguously assigned to the forbidden S_0 ($1^1A_g^-$) → S_1 ($2^1A_g^-$) transition. Ultrafast time-resolved fluorescence and transient absorption experiments were performed to examine the excited state lifetimes and energy state complexion of deoxyperidinin to be compared with the same data obtained from peridinin.[31] Also, quantum computations were carried out to provide a theoretical perspective on the experimental findings. The results give insight into why Nature expended the considerable energy required to produce the highly substituted peridinin molecule as one of its preeminent light-harvesting pigments in photosynthesis.

DOI: 10.1021/acs.jpcb.6b00439
J. Phys. Chem. B 2016, 120, 2731−2744

MATERIALS AND METHODS

Sample Preparation. Samples were purified using a Waters high-performance liquid chromatography (HPLC) instrument equipped with a Waters Atlantis T3 OBD prep column (19 × 100 mm, 5 μm particle size) and a Waters 2996 photodiode array detector prior to the spectroscopic measurements. The mobile phase was acetonitrile delivered isocratically at 2.0 mL/min. For the spectroscopic experiments at room temperature, the molecules were dissolved in either *n*-hexane or acetonitrile (both from Thermo-Fisher Scientific, Pittsburgh, PA). For the experiments at 77 K, the molecules were dissolved in 2-methyltetrahydrofuran (2-MTHF, Sigma-Aldrich, St. Louis, MO), which forms a clear glass at cryogenic temperatures.

Steady-State Spectroscopy. Room temperature absorption spectra were measured using a Varian Cary 50 UV/vis spectrophotometer. Fluorescence spectroscopy was performed at room temperature and 77 K using a Horiba Jobin-Yvon Fluorolog-3 fluorometer. A custom-built liquid nitrogen immersion Dewar was used for the low temperature experiments.

Time-Resolved Fluorescence Spectroscopy. Time-resolved fluorescence (TRF) experiments were carried out using a Hamamatsu universal streak camera setup described previously.[31] The frequency of the excitation pulses was 80 MHz which corresponds to ∼12 ns between subsequent pulses. The depolarized excitation beam was set to 510 nm to excite into the long-wavelength tail region of the $S_0 \rightarrow S_2$ absorption band of deoxyperidinin. The excitation beam had a power of 2.5 mW focused on the sample in a circular spot of ∼1 mm diameter. This corresponded to a photon intensity of $\sim 4 \times 10^{10}$ photons/cm^2 per pulse. The sample absorbance was adjusted to ∼0.3 in a 1 cm cuvette. The emission was measured at a right angle to the excitation beam, and a long-pass 530 nm filter was placed at the entrance slit to the detector to minimize the detection of scattered light from the excitation beam. For the measurements performed at room temperature, the sample was constantly mixed using a magnetic stirrer. The 77 K measurements were carried out using a model SVP-100 liquid nitrogen cryostat (Janis, Woburn, MA, USA) and a 1 cm^2 cryogenic quartz cuvette (NSG Precision Cells, USA). The integrity of the sample was assayed by observing the photon counts to ensure that they were constant over the time course of the experiment, which indicated the absence of photodegradation.

Time-Resolved Absorption Spectroscopy. Transient absorption (TA) measurements were performed using an EOS-Helios TA spectrometer (UltrafastSystems LCC, Sarasota, FL, USA) coupled to a Spectra-Physics femtosecond laser system. The system consists of a Solstice one-box ultrafast amplifier (Spitfire Pro XP, a Ti:sapphire regenerative amplifier with a pulse stretcher and compressor, Mai-Tai, a femtosecond oscillator as the seed source and Empower, a diode-pumped solid state pulsed green laser as the pump source) that produces pulses centered at 800 nm with an energy of ∼3.5 mJ, a ∼90 fs duration, and a 1 kHz repetition rate. The output beam was split with 90% of the light being used to generate a pump beam for the Topas-Prime, an optical parametric amplifier (Light Conversion Ltd., Lithuania). The remaining 10% was used to produce probe pulses in the Helios-EOS spectrometer. The white light continuum probe in the visible (VIS) region was generated by a 3 mm thickness CaF_2 plate. The near-infrared (NIR) probe was generated using a 10 mm thickness proprietary crystalloid rod. A complementary metal−oxide−semiconductor (CMOS) linear sensor with 1024 pixels was used as a detector in the VIS range, and a 256 pixel InGaAs linear diode array was used in the NIR. To provide an isotropic excitation of the sample and avoid pump−probe polarization effects, the pump beam was depolarized. For the room temperature measurements, the energy of the pump beam was set to 1 μJ with a spot size of 1 mm diameter, corresponding to an intensity of $\sim 3 \times 10^{14}$ photons/cm^2, and the sample was stirred continuously using a magnetic stirrer. In order to minimize sample photobleaching at 77 K, the energy of the pump was kept at 0.1 μJ, corresponding to an intensity of 3×10^{13} photons/cm^2. The samples were adjusted to an absorbance of 0.15 (in *n*-hexane) and 0.4 (in acetonitrile) at the absorption maximum (λ_{max}) of the absorption band in a 2 mm path length cuvette and to ∼0.3 for the experiments carried out at 77 K (in 2-MTHF).

Theoretical Methods. Excited state calculations were carried out using a variety of molecular orbital (MO) methods for comparative purposes. Modified neglect of differential overlap with partial single- and double-configuration interaction (MNDO-PSDCI) methods[24,32] were used to explore the oscillator strengths, TA properties, and electron densities of the low-lying singlet states. This semiempirical method includes single and double excitations within the π system and has been useful in understanding the electronic properties of long chain polyenes and carotenoids.[33−35] The standard Austin Model 1 (AM1) parametrization was used, including Mataga repulsion integrals (*rijm* = 2) and identical π and σ electron mobility constants of 1.7 (*pimc* = *sigmc* = 1.7).[24,32] MNDO-PSDCI transition energies are relative to the uncorrelated ground state.[36] Equation-of-motion coupled-cluster with singles and doubles (EOM-CCSD) methods, in addition to the polarizable continuum model (PCM) solvation approach, were used to explore the effect of solvent on the excited state properties.[37−39] The active space of the EOM-CCSD calculations included the 16 highest energy filled and the 16 lowest energy virtual MOs.[40] Excited state properties were calculated relative to the third-order Møller−Plesset (MP3) ground state.[41] Symmetry-adapted-clustered-configuration-interaction (SAC-CI) calculations were carried out at high precision [full single CI and extensive double CI (LevelThree selection)].[42−45] The MNDO-PSDCI calculations were carried out using our own program, and the programs are available by contacting R.R.B. (rbirge@uconn.edu). The *ab initio* and density functional calculations were carried out using Gaussian 09.[46] Ground state density functional calculations used the B3LYP functional and the 6-31G(d) basis set. The excited state calculations used the double-ζ D95 basis set.[47]

RESULTS

Steady-State Spectroscopy. Steady-state absorption spectra of peridinin and deoxyperidinin recorded in *n*-hexane and acetonitrile at room temperature and in 2-MTHF at 77 K are shown in Figure 2. Due to the absence of a carbonyl group in deoxyperidinin that would extend the conjugation of the π-electron system, the absorption spectra are shifted to shorter wavelength by ∼18 nm compared to those of peridinin in the same solvent. In the nonpolar solvent, *n*-hexane, the absorption spectral line shapes of both peridinin and deoxyperidinin exhibit three resolved vibronic bands. These features become less pronounced for peridinin in the polar solvent, acetonitrile, due to inhomogeneous broadening induced by the solvent shell

DOI: 10.1021/acs.jpcb.6b00439
J. Phys. Chem. B 2016, 120, 2731−2744

that takes on many different configurations in the vicinity of the end functional groups, particularly in the region of the lactone ring carbonyl.[24,48] This is not the case for deoxyperidinin, whose absorption spectral profile is only slightly affected by increasing the solvent polarity. This is most likely because the absence of a carbonyl group in the conjugated system narrows the distribution of molecular conformers that can lead to spectral broadening.

The absorption spectra of peridinin and deoxyperidinin shift only slightly when the molecules are dissolved in acetonitrile compared to *n*-hexane, but upon dissolving the molecules in 2-MTHF and lowering temperature to 77 K, the absorption spectra shift substantially to longer wavelength. This is due to the significant increase in the refractive index of 2-MTHF upon freezing. Note that the vibronic features in the 77 K absorption spectrum of deoxyperidinin (Figure 2, bottom left black trace) become much sharper than those seen for peridinin (Figure 2, bottom left green trace), and new features appear in the absorption spectrum for deoxyperidinin at 520, 540, and 570 nm (note the asterisk in the bottom trace in Figure 2) that were not evident in the spectra taken at room temperature. The degree of enhancement of the vibronic structure of the absorption spectrum at low temperature is typical of that reported for carotenoids lacking carbonyl groups in conjugation with the π-electron polyene chain.[15,34,49−51] In order to confirm that these additional peaks were due to deoxyperidinin and not to impurities, fluorescence excitation spectra were recorded by monitoring the emission of deoxyperidinin over a wide range of wavelengths from 640 to 757 nm. It was found that the additional features were present in all the excitation scans and matched precisely the line shape of the $1 - T$ (where T is transmittance) spectrum of deoxyperidinin. (See the bottom of Figure 2 for an overlay of the $1 - T$ spectrum (black trace) with the excitation spectrum (red dashed trace) detected at 689 nm.) These experiments confirm that these absorption features belong to deoxyperidinin, and their wavelength position being in close proximity to the well-resolved $S_1 \rightarrow S_0$ emission spectrum shown in Figure 2 is indicative of the peaks being assigned to the $S_0 \rightarrow S_1$ absorption transition of this molecule.

Fluorescence spectra of peridinin and deoxyperidinin are also shown in Figure 2. For both molecules, the spectra are substantially red-shifted relative to their respective absorption profiles. This is a clear indication that the emission originates primarily from the S_1 state rather than the S_2 state. Similar to the absorption spectra, the fluorescence spectral line shapes of both molecules recorded in *n*-hexane exhibit clear vibronic features. These features disappear for the spectrum of peridinin recorded in acetonitrile due to conformational disorder induced by the presence of the carbonyl group but remain for deoxyperidinin in that solvent because it has no carbonyl group in conjugation. Moreover, the wavelength position of the fluorescence spectrum of deoxyperidinin remains essentially constant upon changing the solvent, whereas that of peridinin shifts substantially to longer wavelengths when the molecule is dissolved in acetonitrile.

Time-Resolved Fluorescence Spectroscopy. Contour surfaces representing the TRF spectra of deoxyperidinin recorded in *n*-hexane and acetonitrile at room temperature and in 2-MTHF at 77 K are shown in Figure 3. The samples were excited at 510 nm, which corresponds to the long-wavelength edge of the 0−0 vibronic band of the $S_0 \rightarrow S_2$ absorption. Consistent with the results from the steady-state fluorescence experiments described above, the dominant signal

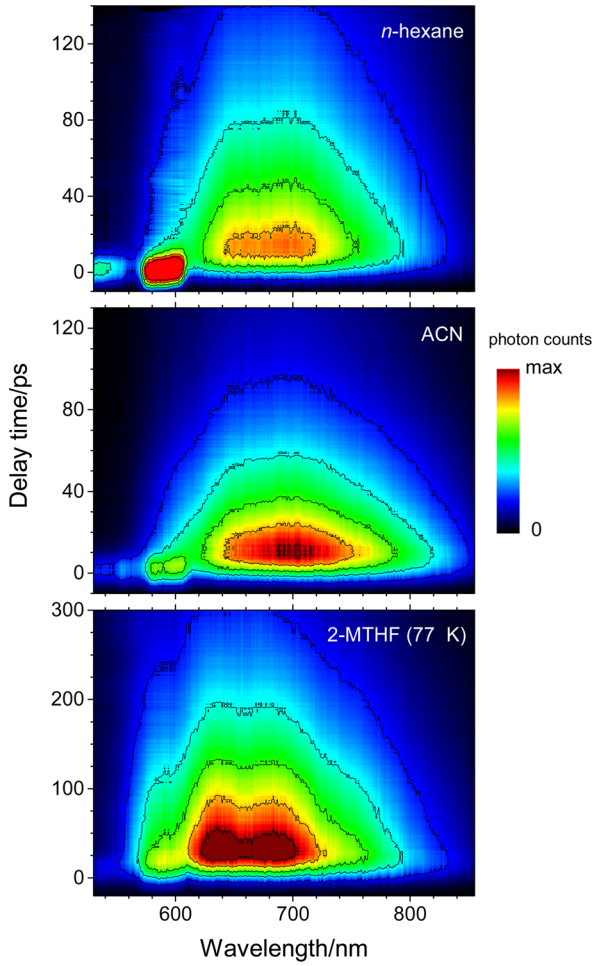

Figure 3. Contour surfaces of TRF spectra of deoxyperidinin recorded in *n*-hexane and ACN at room temperature and 2-MTHF at 77 K after excitation at 510 nm corresponding to the long-wavelength edge of the (0−0) vibronic band of the S_0 ($1^1A_g^-$) → S_2 ($1^1B_u^+$) absorption band. The dominant signal is associated with fluorescence from the S_1 ($2^1A_g^-$) state. At early delay times, the S_1 ($2^1A_g^-$) emission signal is obscured by overlapping emission from the S_2 ($1^1B_u^+$) state and a strong solvent Raman band at ∼580 nm.

is associated with fluorescence from the S_1 state. In fact, if all the TRF spectra are summed, the resulting profile will reproduce the steady-state fluorescence spectrum shown in Figure 2. At early delay times, however, the S_1 emission signal is obscured by overlapping emission from the short-lived S_2 state and a solvent Raman band at ∼580 nm. Thus, TRF experiments along with global analysis provide a way of obtaining fluorescence spectra originating from the S_1 state separate from fluorescence bands associated with emission from the S_2 state. These "pure" $S_1 \rightarrow S_0$ fluorescence spectra are given in Figure 4A−C as evolution associated spectra (EAS), so-named because they result from a global analysis employing a two-component sequential decay path model.[52] In Figure 4A−C, only the EAS profile associated with the longer-lived of the two components is shown. The short-lived component consisting of Raman bands and the long-wavelength tailing edge of the $S_2 \rightarrow S_0$ emission spectra are omitted from the figure for clarity.

The right-hand side panels of Figure 4 represent kinetic traces extracted from the data at the indicated wavelengths overlaid with the fits obtained from global analysis. The

DOI: 10.1021/acs.jpcb.6b00439
J. Phys. Chem. B 2016, 120, 2731−2744

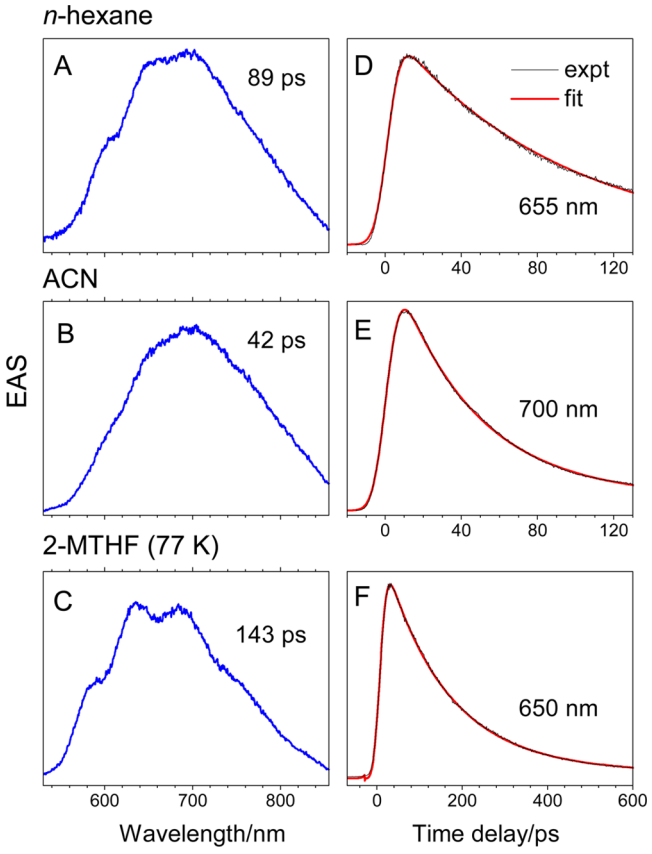

Figure 4. Global analysis of fluorescence decay contours. (A–C) Evolution associated spectra (EAS) corresponding to fluorescence from the S_1 ($2^1A_g^-$) state only with the lifetime of the component indicated. Shorter-lived components associated with the tail of the S_2 ($1^1B_u^+$) emission and an intense Raman band due to the solvent were omitted for clarity. (D–F) Representative kinetic traces for the decay of the S_1 ($2^1A_g^-$) → S_0 ($1^1A_g^-$) fluorescence recorded at the specified wavelengths. The experimental traces (black lines) are overlaid with the fits from the global analysis (red lines).

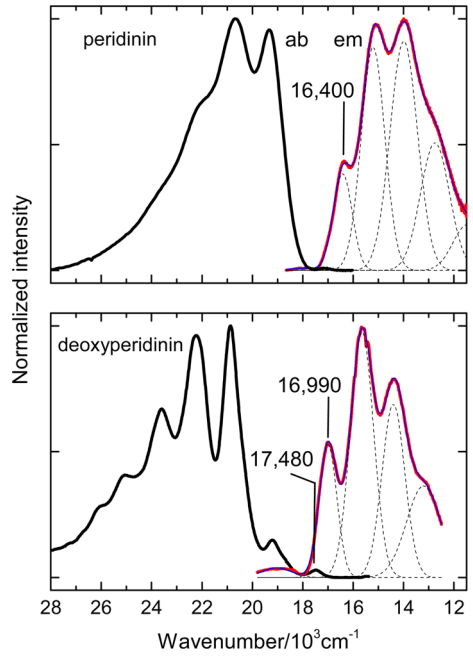

Figure 5. Spectral reconstruction (red traces) of the experimental S_1 ($2^1A_g^-$) → S_0 ($1^1A_g^-$) emission profile (right black traces) of peridinin (top panel) and deoxyperidinin (bottom panel) recorded in 2-MTHF at 77 K and reconstructed using Gaussian line shapes corresponding to vibronic bands (dashed traces). A comparison with the absorption spectra (left black trace) also recorded in 2-MTHF at 77 K shows that the (0–0) vibronic band of the small low energy feature in the absorption spectrum of deoxyperidinin appearing at 17 480 cm^{-1} is separated by only 490 cm^{-1} from the high energy (0–0) vibronic band appearing at 16 990 cm^{-1} in the emission spectrum, suggesting they correspond to the same electronic transition.

fluorescence lifetimes are also indicated in the left-hand panels of Figure 4 and reveal an effect of solvent on the dynamics of the S_1 state of deoxyperidinin. The lifetime is 89 ps in *n*-hexane but decreases to 42 ps in the polar solvent, methanol. At 77 K in 2-MTHF, the lifetime is increased substantially to 143 ps.

In order to obtain a precise measurement of the S_1 state energy of deoxyperidinin, its 77 K emission spectrum was reconstructed by summing five independent Gaussian functions (Figure 5). The analysis was facilitated by the relatively high degree of vibronic resolution displayed by the emission spectral line shape. The fitting provided a measurement of the apparent Stokes shift between the lowest energy vibronic feature in the absorption spectrum found to be 17 480 cm^{-1} and the highest energy vibronic band in the fluorescence spectrum, which was determined by the fitting to be 16 990 cm^{-1}. The difference of 490 cm^{-1} between these two values is a typical Stokes shift for carotenoids.[13] Thus, the energy of the S_1 state of deoxyperidinin can be taken to be 17 240 ± 250 cm^{-1}, which represents the average of the two values along with the range spanned by them as the uncertainty in the measurement. In comparison, the lowest energy vibronic band in the absorption spectrum of peridinin recorded in 2-MTHF at 77 K has been reported to be 17 020 cm^{-1}, and the highest energy vibronic band in the fluorescence spectrum was found to be 16 400 cm^{-1} (Figure 5).[27] The average and range spanned by these two values yields 16 710 ± 310 cm^{-1}, which can be taken as the S_1 energy of peridinin recorded under these same experimental conditions to be compared with that of deoxyperidinin. The fact that the corresponding value from deoxyperidinin is higher by 530 cm^{-1} is due to the absence of the carbonyl group in the lactone ring (Figure 1), which restricts π-electron delocalization and raises the energy of its S_1 state compared to that of peridinin.

Transient Absorption Spectroscopy. TA spectra of deoxyperidinin dissolved in *n*-hexane and acetonitrile at room temperature and 2-MTHF at 77 K and recorded in the visible and near-infrared (NIR) regions at various time delays are shown in Figure 6. The samples were excited into the 0–0 band of the $S_0 \rightarrow S_2$ absorption transition. After laser excitation, the transient spectra show a rapid onset of bleaching of the steady-state absorption in the 400–500 nm wavelength region along with a buildup of a fairly narrow excited state absorption (ESA) band at ~500 nm that can be attributed to a strongly allowed S_1 ($2^1A_g^-$) → S_n ($^1B_u^+$) transition. Both the bleaching and the ESA band decay concomitantly in tens of picoseconds. These spectral features and kinetic behavior are typical of carotenoids.[53] What is unusual about the spectra, and not normally seen for carotenoids, is the appearance of an additional low energy ESA transition at 660 nm in *n*-hexane, 650 nm in acetonitrile, and 700 nm in 2-MTHF (at 77 K). It is important to point out that this ESA band is not exactly the same as that reported for peridinin and other carbonyl-containing carotenoids in this wavelength region and which has been assigned to a transition from an intramolecular charge

DOI: 10.1021/acs.jpcb.6b00439
J. Phys. Chem. B 2016, 120, 2731–2744

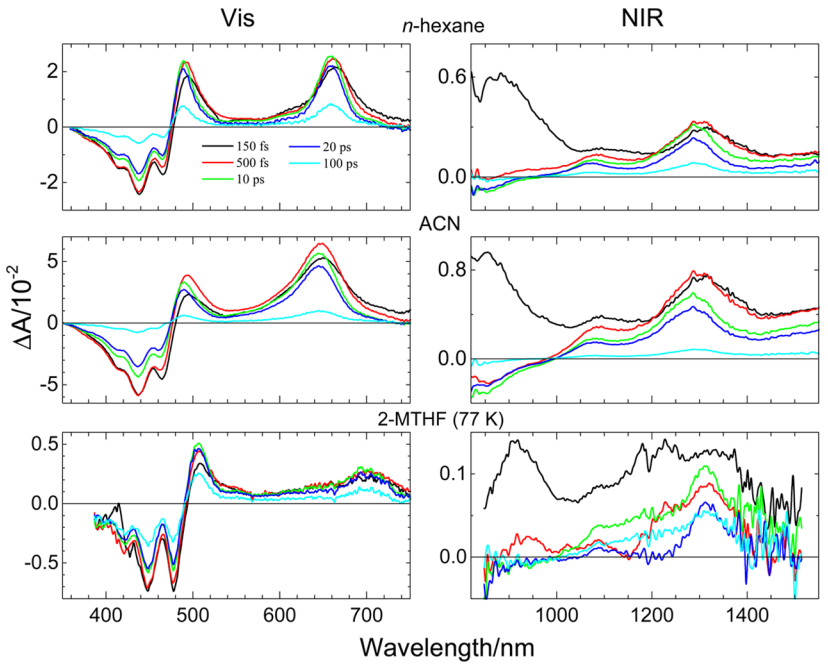

Figure 6. Transient absorption of deoxyperidinin in *n*-hexane and ACN at room temperature and in 2-MTHF at 77 K recorded in the visible and NIR spectral ranges.

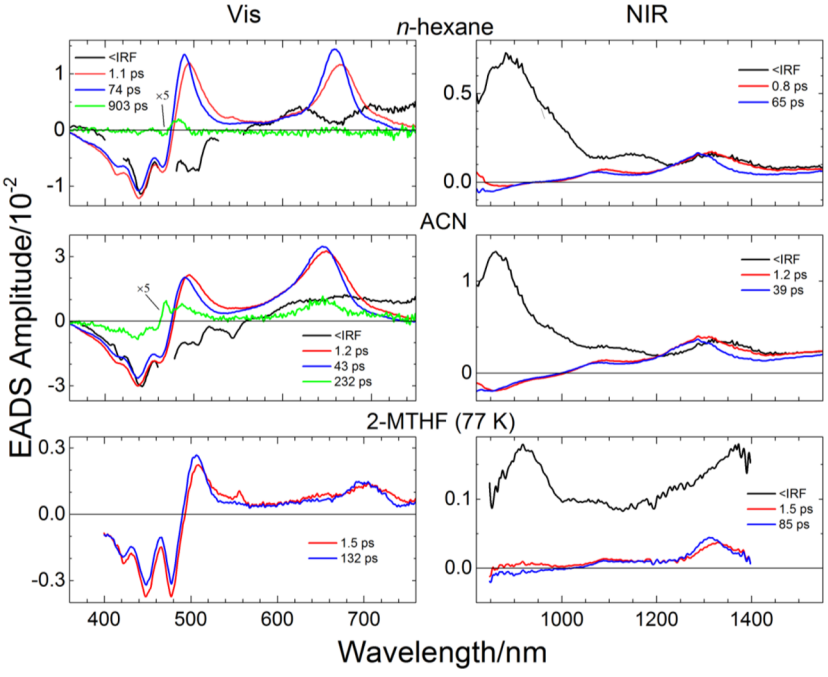

Figure 7. Evolution associated difference spectra (EADS) based on global fitting the transient absorption data sets of deoxyperidinin illustrated in Figure 6 to a sequential decay model.

transfer (ICT) state to a higher (S_n) singlet state. The ICT → S_n transition in peridinin is much broader than the low energy ESA band seen here for deoxyperidinin, exhibits a profound effect of solvent polarity on both the high energy and lower energy ESA bands in the TA spectrum, and decays with different kinetics than the S_1 ($2^1A_g^-$) → S_n ($n^1B_u^+$) transition.[26,27,29,54−56] The narrowness of this low energy ESA band for deoxyperidinin, its similarity in width and amplitude to the higher energy S_1 ($2^1A_g^-$) → S_n ($n^1B_u^+$) transition, and the fact that it decays with the same kinetics as the higher energy ESA band suggest that the transition originates from the S_1 ($2^1A_g^-$) state and terminates at a different, lower-lying B_u^+ state than that for the higher energy ESA band observed at ∼500 nm. The low energy ESA band mirrors the behavior of the S_0 ($1^1A_g^-$) → S_2 ($1^1B_u^+$) steady-state spectra (Figure 2) both in that it shifts only slightly when the molecule is dissolved in acetonitrile compared to *n*-hexane and that it shifts substantially to longer wavelength when the spectrum is recorded using 2-MTHF at 77 K (Figure 6). The observation that the low energy ESA feature decreases in

DOI: 10.1021/acs.jpcb.6b00439
J. Phys. Chem. B 2016, 120, 2731−2744

intensity relative to the higher energy S_1 ($2^1A_g^-$) → S_n ($n^1B_u^+$) band in the spectrum recorded at 77 K may indicate that, at low temperatures, conformations of the molecule associated with a lower oscillator strength of the transition are frozen in preferentially.

The TA spectra recorded in the NIR region (right-hand panels in Figure 6) show a band at ~900 nm that occurs at very early delay times and decays within the time profile of the instrument response function. This strongly suggests that it be assigned to ESA between the S_2 ($1^1B_u^+$) state and a higher-lying A_g^- state as reported previously for several polyenes and carotenoids.[49,50,57] Other peaks appearing between 1000 and 1400 nm can be assigned to vibronic bands associated with the S_1 ($2^1A_g^-$) → S_2 ($1^1B_u^+$) transition.[49,50,58−60] However, because the energy separation between the S_1 ($2^1A_g^-$) and S_2 ($1^1B_u^+$) states is estimated to be 3840 cm^{-1} from the difference in the (0−0) vibronic bands of the S_0 ($1^1A_g^-$) → S_2 ($1^1B_u^+$) absorption spectrum (20 830 cm^{-1} based on the (0−0) band in Figure 5) and the S_1 ($2^1A_g^-$) → S_0 ($1^1A_g^-$) fluorescence spectrum (16 990 cm^{-1}; see above and Figure 5) recorded in 2-MTHF at 77 K, these vibronic features in the NIR spectra must then be associated with transitions from the lowest vibronic level of the S_1 ($2^1A_g^-$) state to higher vibronic levels of the S_2 ($1^1B_u^+$) state; i.e., the (0−0) band of the S_1 ($2^1A_g^-$) → S_2 ($1^1B_u^+$) transition is well out of the range of the TA spectrometer detection system.

In order to obtain more detailed information regarding the dynamics of the excited states of deoxyperidinin, global analysis of the spectral and temporal data sets in the visible and NIR regions was carried out based on a sequential decay model. This type of fitting results in evolution associated difference spectra (EADS) that are shown in Figure 7. In all cases, the best fit was determined by a minimization of the residuals and a consideration of the resulting χ^2 value. The high quality of the analysis is illustrated by representative kinetic traces and their associated fits given in Figure 8.

For the data sets recorded at room temperature, four components were required to achieve a good fit for the data in the visible region, and three components were needed for the data in the NIR. The fastest EADS components (black lines in Figure 7) are associated with the lifetime of the S_2 ($1^1B_u^+$) excited state. This is evidenced by the rapid bleaching of the S_0 ($1^1A_g^-$) → S_2 ($1^1B_u^+$) steady-state absorption and stimulated emission in the visible region, and the immediate appearance (and rapid decay) of the S_2 ($1^1B_u^+$) → S_n transition in the NIR. The second EADS component (red lines in Figure 7) decayed in times ranging from 0.8 to 1.5 ps. On the basis of these values and the narrowing of the profiles that occurs when this second EADS decays into a third EADS (blue lines in Figure 7), the lifetime of the second component can be assigned to vibronic equilibration in the S_1 state. The third EADS represents the lifetime of the relaxed S_1 ($2^1A_g^-$) state. The value is essentially the same from data in the visible region compared to that obtained from data in the NIR region for a given solvent, and it ranges between 39 and 74 ps based on the room temperature data sets (Table 1). It is longer at 132 ps (fit to the visible data set) or 85 ps (fit to the NIR data set) for the measurements done at 77 K. The final component obtained in the fits to the visible data sets taken for the molecule dissolved in *n*-hexane and acetonitrile (green traces in Figure 7) has a very low amplitude and a long lifetime. On the basis of these observations, and the fact that the spectral feature is shifted to shorter wavelength than the large amplitude associated with

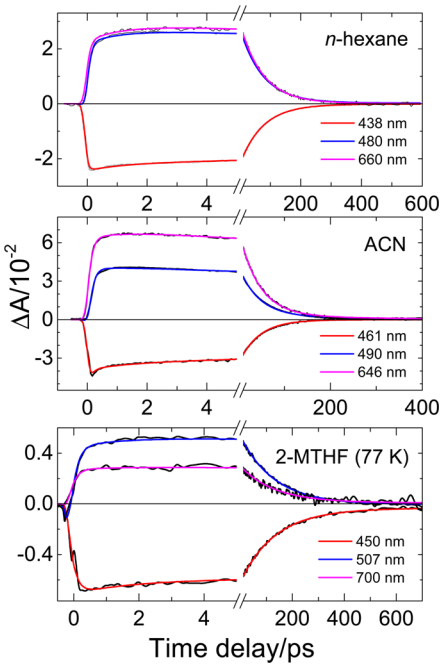

Figure 8. Representative kinetic traces extracted from the global analysis of the transient absorption data sets at selected wavelengths from deoxyperidinin recorded in *n*-hexane and ACN at room temperature and in 2-MTHF at 77 K.

Table 1. Dynamics of the Excited States of Deoxyperidinin in Various Solvents Obtained from the Global Fitting of Transient Absorption (TA) and Time-Resolved Fluorescence (TRF) Data Set[a]

		TA lifetime (ps)				TRF lifetime (ps)	
solvent	probe	τ_1	τ_2	τ_3	τ_4	τ_{F1}	τ_{F2}
n-hexane	vis	<IRF	1.1	74	903	<IRF	89
	NIR	<IRF	0.8	65			
acetonitrile	vis	<IRF	1.2	43	232	<IRF	42
	NIR	<IRF	1.2	39			
2-MTHF (77 K)	vis	<IRF	1.5	132	n.e.	<IRF	143
	NIR	<IRF	1.5	85			

[a]<IRF, dynamics are faster than or comparable to the instrument response function; n.e., not evident; τ_4 is very likely the kinetic component associated with a rapidly decaying triplet state formed via singlet fission which subsequently annihilates.

the S_1 ($2^1A_g^-$) → S_n ($n^1B_u^+$) transition, this final component can be assigned to the decay of a triplet−triplet absorption transition. Triplet formation may occur due to singlet−triplet intersystem crossing, but this process happens with extremely low yield.[27,61] All of the kinetic parameters obtained from the global analysis fits are summarized in Table 1.

DISCUSSION

The absence of the carbonyl group in deoxyperidinin compared to peridinin results in a narrowing of the absorption and fluorescence spectral features which can be accounted for on the basis of a substantial reduction in the distribution of conformational isomers in solution.[62] The narrowing of the line shape for deoxyperidinin provided an added benefit for experiments carried out at 77 K, in which features in its steady-state absorption spectrum (Figures 2 and 5) can be

DOI: 10.1021/acs.jpcb.6b00439
J. Phys. Chem. B 2016, 120, 2731−2744

unambiguously assigned to the forbidden S_0 ($1^1A_g^-$) → S_1 ($2^1A_g^-$) transition.

The lack of a carbonyl group in deoxyperidinin precludes the formation of an ICT state, which is only expected to be formed in polyenes and carotenoids, such as peridinin, which possess a carbonyl functional group in conjugation with the π-electron chain.[15,62] For peridinin, the large dipole moment associated with its charge transfer character gives rise to broader steady-state absorption and fluorescence spectra compared to those from molecules lacking carbonyl functional groups. This is particularly evident when the molecules are dissolved in polar solvents (Figure 2). Moreover, a profound effect of solvent polarity on the S_1 ($2^1A_g^-$) lifetime has been reported for several carbonyl-containing carotenoids and polyenes.[15,30,62] For example, when peridinin is dissolved in *n*-hexane, the S_1 ($2^1A_g^-$) lifetime is 161 ps. The value decreases by more than an order of magnitude to 9 ps when the molecule is dissolved in acetonitrile.[15] Thus, the lack of a carbonyl group in deoxyperidinin makes it somewhat surprising that the S_1 lifetime of that molecule also depends on solvent polarity, although the effect is not as large as that reported for peridinin. The S_1 ($2^1A_g^-$) lifetime of deoxyperidinin was found here to be 89 ps (TRF) and 74 ps (TA) for the molecule dissolved in *n*-hexane. The lifetime is shortened by an approximate factor of 2 for deoxyperidinin dissolved in acetonitrile; the values are 42 ps (TRF) or 43 ps (TA). For the molecule dissolved in 2-MTHF and experiments done at 77 K, the S_1 lifetime lengthens to 143 ps (TRF) and 132 ps (TA). Also, in the TA spectra of deoxyperidinin in *n*-hexane and acetonitrile recorded in the NIR (Figure 6), a negative signal due to stimulated emission is observed between 900 and 1000 nm, which for peridinin has been associated with the formation of an ICT state preferentially in polar solvents.[53] For deoxyperidinin, the fact that the signal is present in both polar and nonpolar solvents (Figure 6) and that it decays with the same lifetime as the S_1 ($2^1A_g^-$) state (Figure 7) indicates that it is not due to an ICT state, despite the fact that the signal is slightly larger in acetonitrile compared to *n*-hexane. The most likely reason for the appearance of the signal is the fact that the oscillator strength of the S_1 ($2^1A_g^-$) → S_0 ($1^1A_g^-$) transition is gained by mixing $^1B_u^+$ character into the lowest lying S_1 ($2^1A_g^-$) state. This is also the case for peridinin, but its effect is masked in polar solvents by strong stimulated emission from the ICT state. Quantum computations presented below support this view.

A reasonable interpretation for the decrease in the S_1 lifetime with increasing solvent polarity is the possibility that the polar solvent enhances vibrational−electronic coupling between the S_1 and ground states of multiple conformers formed in the polar solvent, which would lead to an increased rate of internal conversion, and, as a consequence, a shorter S_1 ($2^1A_g^-$) state lifetime compared to that observed in the nonpolar solvent. At 77 K, the opposite is true. The low temperature narrows the distribution of conformers (evidenced by narrowing of the steady-state absorption and fluorescence spectral line widths, Figure 2), limits the number of promoting vibrational modes for internal conversion, and reduces the vibrational−electronic coupling between the S_1 and S_0 states which ultimately results in lengthening the S_1 lifetime.

A remarkable observation reported here is that the S_0 ($1^1A_g^-$) → S_1 ($2^1A_g^-$) transition is clearly evident for deoxyperidinin, especially at 77 K (Figures 2 and 5), but is hardly noticeable for peridinin (Figure 2). The lack of the carbonyl group from the lactone ring of deoxyperidinin is the key to understanding this issue.

A spectral feature that distinguishes the TA spectrum of deoxyperidinin from that of peridinin is a low-energy transition occurring between 650 and 700 nm (Figure 6). Unlike the TA spectrum for peridinin in this region that has been associated with an ICT → S_n transition and which exhibits a profound effect of solvent on amplitude and kinetics, the band for deoxyperidinin is hardly affected by solvent polarity and has a similar line width, intensity, and dynamics as the standard S_1 ($2^1A_g^-$) → S_n ($n^1B_u^+$) transition which appears at ∼500 nm (Figure 6). This suggests that it also originates from the S_1 ($2^1A_g^-$) state and terminates in a lower-lying $^1B_u^+$ state. A low-energy TA band with these characteristics has never been reported for any carotenoid.

Theoretical calculations were carried out to help explain this aspect and the other photophysical properties of deoxyperidinin in comparison to those observed in peridinin. Contrary to intuition, replacing the lactone carbonyl group of peridinin with two hydrogen atoms generates a chromophore that retains a large dipole moment (Figure 1). In fact, when the full system is calculated, deoxyperidinin has a larger dipole moment than peridinin. However, the directions of the dipole moments in the two molecules are significantly different (Figure 1). These relative characteristics are retained in the C_s model chromophores of peridinin (denoted "percs" in Figure 1) and deoxyperidinin (denoted "deoxypercs" in Figure 1). The origin of the anomalously large dipole moment of deoxyperidinin can be understood with reference to the dipole moments of the isolated ring systems, as shown in Figure 9. Long chain

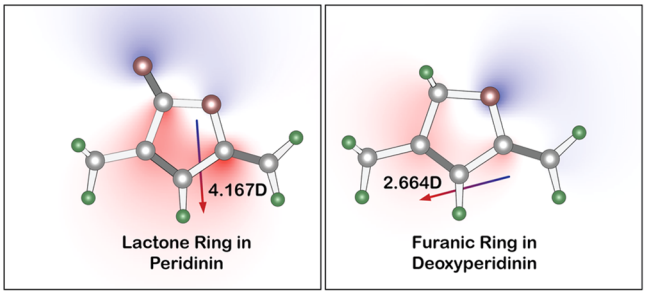

Figure 9. Comparison of the dipolar properties of the isolated lactone ring of peridinin and the isolated furanic ring of deoxyperidinin based on density functional theory [B3LYP/6-31G(d)].

polyenes have a large polarizability along the main axis and a much smaller polarizability orthogonal to the main axis. The dipole moment of the lactone ring of peridinin is orthogonal to the main axis, whereas the dipole moment of the furanic ring of deoxyperidinin is within 20° of the main axis of the polyene. This observation means that the furanic ring of deoxyperidinin can induce a much larger dipole moment on the polyene than can the lactone ring of peridinin. Induced dipole moments are only part of the story because the two oxygen atoms in the lactone ring of peridinin have a combined negative charge of −0.996, whereas the single oxygen in the furanic ring in deoxyperidinin has a negative charge of −0.533. Thus, the lactone ring extracts more negative charge from the polyene chain than does the furanic ring of deoxyperidinin. The large dipole moment of peridinin is due primarily to charge induction (electronegativity) effects, whereas the large dipole moment of deoxyperidinin is due primarily to induced dipole effects. It is

DOI: 10.1021/acs.jpcb.6b00439
J. Phys. Chem. B 2016, 120, 2731−2744

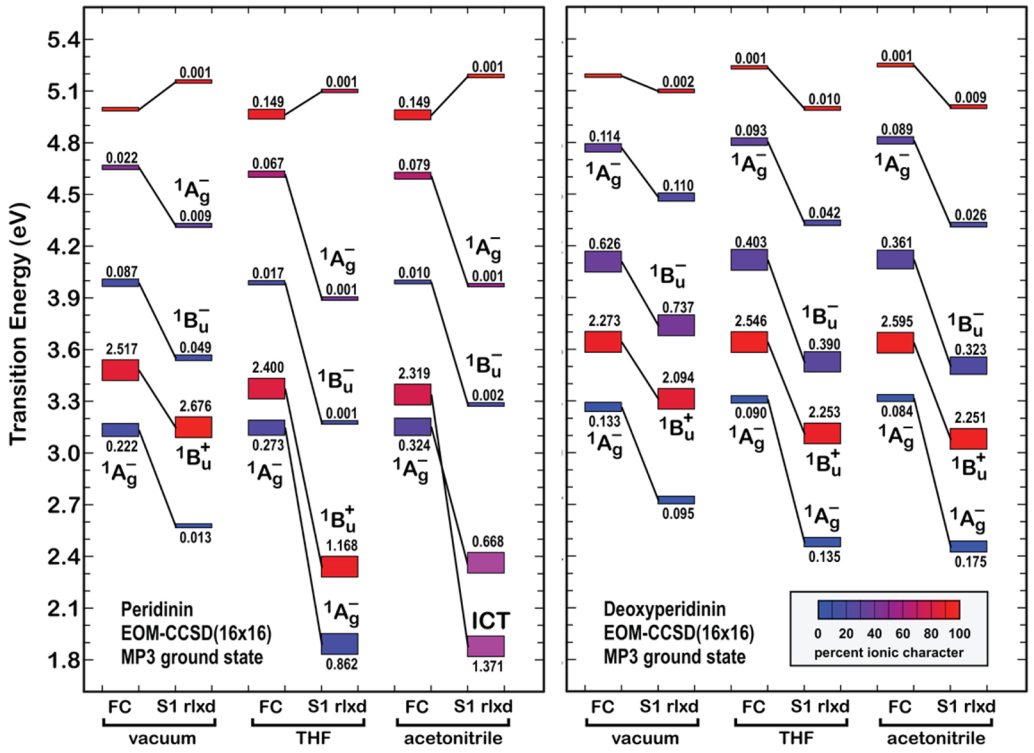

Figure 10. Effect of solvent environment on the lowest excited Franck–Condon (FC) and relaxed (S1 rlxd) singlet states of the simplified chromophore of peridinin (percs, left panel) and deoxyperidinin (deoxypercs, right panel) based on EOM-CCSD procedures. Transition energies are relative to the MP3 ground state. Solvent polarity increases from left to right, but the leftmost pair in each panel is for vacuum conditions. The symmetry labels are approximate.

the difference in the directions of the two dipole moments that play an important role in the photophysical properties of these two molecules.

The first theoretical goal is to explain why the forbidden S_0 $(1^1A_g^-) \rightarrow S_1$ $(2^1A_g^-)$ transition is clearly observable in the absorption spectrum of deoxyperidinin but virtually spectroscopically silent for peridinin (Figures 2 and 5). EOM-CCSD calculations were first carried out to explore the observation of the forbidden S_0 $(1^1A_g^-) \rightarrow S_1$ $(2^1A_g^-)$ transition. Note that the simplified models of deoxyperidinin and peridinin (deoxypercs and percs in Figure 1) were used in the calculations to reduce the computational time and to make the EOM-CCSD calculations tractable. This efficiency is achieved via two mechanisms. First, the number of atoms decreases from 96 (or 97) to 45 (or 46). Of equal importance is the fact that the model chromophores have C_s symmetry, which allows the CI matrices to be handled in symmetry blocks. For the vacuum conditions presented in Figure 10, EOM-CCSD calculations predict that deoxyperidinin has a lower S_0 $(1^1A_g^-) \rightarrow S_1$ $(2^1A_g^-)$ oscillator strength than peridinin, where $f(2^1A_g^-)/f(1^1B_u^+) = 0.133/2.273 = 0.058$ in deoxyperidinin (Franck–Condon (FC) geometry, deoxypercs) but $f(2^1A_g^-)/f(1^1B_u^+) = 0.222/2.517 = 0.088$ in peridinin (FC geometry, percs). Furthermore, with increased solvent polarity, the S_0 $(1^1A_g^-) \rightarrow S_1$ $(2^1A_g^-)$ transition is predicted to have an increased oscillator strength in peridinin and a decreased oscillator strength in deoxyperidinin. A more careful examination of the results, however, indicates that EOM-CCSD predicts a much larger energy gap between the $2^1A_g^-$ and $1^1B_u^+$ states in deoxyperidinin, particularly in polar solvents. Increased separation will render the S_0 $(1^1A_g^-) \rightarrow S_1$ $(2^1A_g^-)$ transition better resolved in the spectral region where the long-wavelength tail of the strongly allowed S_0 $(1^1A_g^-) \rightarrow S_2$ $(1^1B_u^+)$ transition has the potential to mask the weaker spectral features associated with the forbidden transition.

However, inhomogeneous broadening is a mechanism that also must be taken into account. In fact, it may be more important in enhancing the observed vibronic development of the S_0 $(1^1A_g^-) \rightarrow S_1$ $(2^1A_g^-)$ transition. As can be seen in the absorption and fluorescence spectra of Figures 2 and 5, the vibronic bands of deoxyperidinin are sharper than those observed for peridinin. Given that the ground state dipole moments are comparable, this observation requires a thorough examination because the origin of the inhomogeneous broadening is not obvious. There are two principal mechanisms of inhomogeneous broadening typically observed in polar polyenes. One involves a ground state degree of freedom that has a broad potential energy surface that, when explored thermally, results in a range of transition energies that fills in the absorption spectrum. A good example of this feature is observed in the absorption spectra of the retinal chromophores, which are broadened due to rotational freedom involving the β-ionylidene ring.[48] No comparable degree of freedom is present in the compounds studied here. An alternative mechanism is solvent-induced inhomogeneous broadening. This mechanism is associated with a large change in dipole moment or a large shift in the dipole moment direction upon excitation. The mechanism is based on the assumption that an optimal solvent organization in the ground state will not be optimal for the excited state. Thus, small variations in the ground state solvent distribution can create a range of transitions energies that fill in the vibronic distribution and broaden the resulting absorption spectrum. The SAC-CI methods were selected to explore this mechanism because SAC-CI theory provides the highest quality

DOI: 10.1021/acs.jpcb.6b00439
J. Phys. Chem. B 2016, 120, 2731–2744

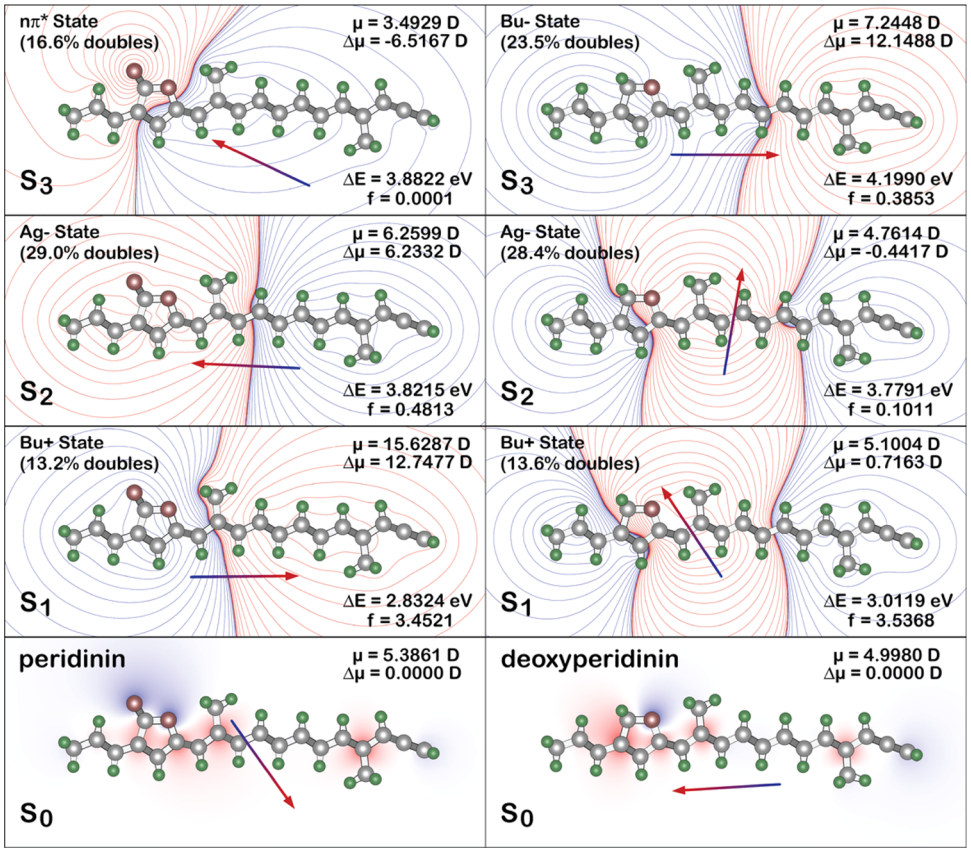

Figure 11. Dipolar properties of the ground state and the three lowest excited singlet states of simplified peridinin (percs, left panels) and simplified deoxyperidinin (deoxypercs, right panels) based on full SAC-CI calculations in vacuum. The dipole moments and magnitude of the vectorial dipole moment changes relative to the ground state are shown in the upper right of each panel. The dipole moment vectors are shown using arrows of arbitrary length using the conventions of Figure 1. The ground state dipole moments are based on the restricted Hartree−Fock SAC-CI calculations using the D95 basis set (see theoretical). These values differ from those of Figure 1 which were based on density functional methods [B3LYP/6-31G(d)]. Note that the $2^1A_g^-$ state is calculated to be above the $1^1B_u^+$ state, which is not consistent with experiments. Nevertheless, the dipole moments are believed to be reliable based on previous studies (see text).

ground and excited state electron densities of the *ab initio* methods available.[63] The SAC-CI methods, however, do suffer from one deficiency when used to explore long chain polyenes. These methods fail to place the $2^1A_g^-$ below the $1^1B_u^+$ state, but the configurational characteristics remain valid and the electron densities and dipole moments are stable and valid for the low-lying states.[35,63] The results of SAC-CI vacuum calculations are shown in Figure 11. The dipole moment changes ($\Delta\mu$) are listed underneath the dipole moments (μ) with both in Debyes (D). The value of the magnitude of the shift vector for S_n is given by

$$\begin{aligned}\Delta\mu_n &= S^{\pm}|\overrightarrow{\Delta\mu_n}| \\ &= S^{\pm}[(\mu_n^{(x)} - \mu_0^{(x)})^2 + (\mu_n^{(y)} - \mu_0^{(y)})^2 \\ &\quad + (\mu_n^{(z)} - \mu_0^{(z)})^2]^{1/2}\end{aligned} \tag{1}$$

where the sign term, $S^{\pm}$, is determined on the basis of the relative direction of the ground and excited state dipole moments. If the vector representing the dipole moment change has a direction within ±90° of the ground state dipole moment vector, the sign is positive; otherwise, it is negative. The contours displayed in the excited state panels in Figure 11 show the magnitude of the charge shift upon excitation with the contours chosen so that roughly 30 contours are displayed for each state. The key observation is that the $2^1A_g^-$ state dipole moment change of deoxyperidinin (S_2 state of the right panel of Figure 11) is only 0.442 D, significantly smaller than the corresponding dipole moment change of 6.233 D in peridinin (S_2 state of the left panel of Figure 11). On the basis of a very simple Onsager reaction field analysis, the line broadening associated with solvent-induced electrostatic inhomogeneous broadening can be estimated using eq 2

$$\Delta E_n = \frac{1}{\sqrt{2}}(\overrightarrow{\Delta\mu_n}\cdot\overrightarrow{\mu_0})\frac{(\varepsilon - 1)}{2\varepsilon + 1}\frac{1}{a_u^3} \tag{2}$$

where ε is the dielectric constant of the solvent, a_u is the cavity radius of the solute, $\overrightarrow{\mu_0}$ is the ground state dipole moment of the solute, and $\overrightarrow{\Delta\mu}$ is the dipole moment difference vector

$$\overrightarrow{\Delta\mu} = (\mu_n^{(x)} - \mu_0^{(x)})\mathbf{i} + (\mu_n^{(y)} - \mu_0^{(y)})\mathbf{j} + (\mu_n^{(z)} - \mu_0^{(z)})\mathbf{k} \tag{3}$$

If the analysis is further simplified by calculating the ratio of the inhomogeneous broadening of two molecules in the same solvent and nearly identical cavity radii, one gets

$$\Delta E_n^{\mathrm{rel}} = \frac{(\overrightarrow{\Delta\mu_n^{(1)}}\cdot\overrightarrow{\mu_0^{(1)}})}{(\overrightarrow{\Delta\mu_n^{(2)}}\cdot\overrightarrow{\mu_0^{(2)}})} \tag{4}$$

DOI: 10.1021/acs.jpcb.6b00439
J. Phys. Chem. B 2016, 120, 2731−2744

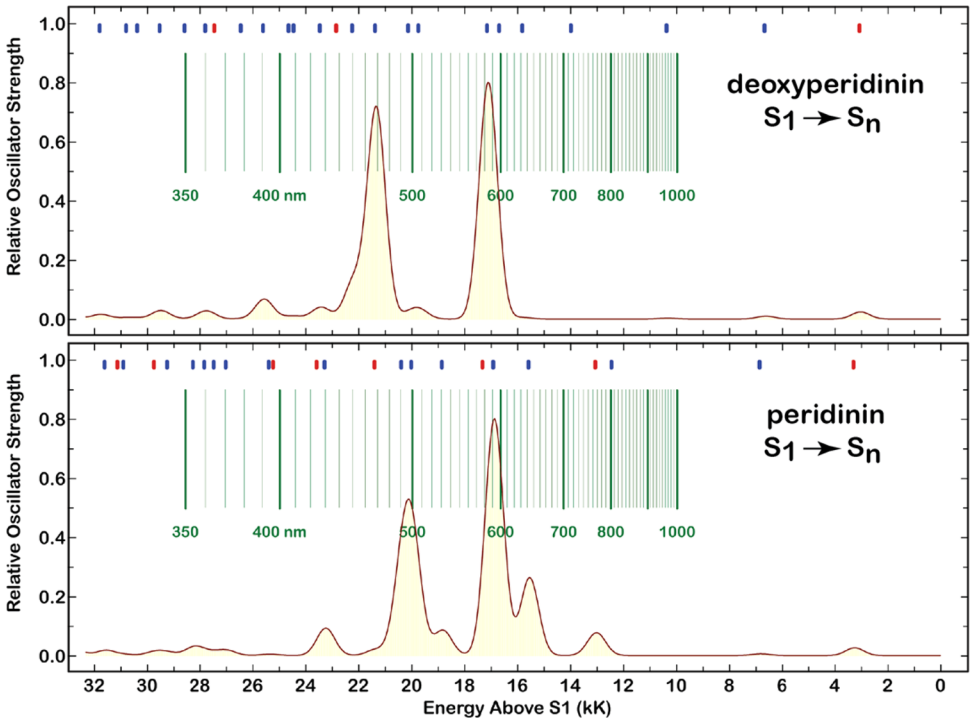

Figure 12. $S_1 \rightarrow S_n$ spectra of simplified peridinin (percs) and simplified deoxyperidinin (deoxypercs) based on MNDO-PSDCI theory. The transitions are shown with artificially narrow bandwidths to help identify the individual transitions responsible. The individual S_n excited states are marked with blue or red bars at the top, where blue indicates a covalent S_n state and red indicates an ionic S_n state. The unit kK equals 1000 cm^{-1}.

The SAC-CI calculations summarized in Figure 11 indicate that the spectra associated with the $2^1A_g^-$ excited state of peridinin will have an ~14-fold larger degree of electrostatic inhomogeneous broadening than observed for those associated with the same state in deoxyperidinin. (The spectra corresponding to the $1^1B_u^+$ states are calculated to have an even larger difference of ~17 in relative inhomogeneous broadening.) These simple calculations help rationalize the relative sharpness of the vibronic bands observed for deoxyperidinin relative to those of peridinin in Figure 5, but it is noticed that the differences are smaller than suggested by these calculations. Thus, there may be other sources of inhomogeneous broadening contributing to the spectra of these molecules, possibly involving thermal rotation around single bonds within the polyene framework.

In summary, the observation of discrete vibronic bands associated with transitions from the ground S_0 ($1^1A_g^-$) state to the S_1 ($2^1A_g^-$) excited singlet state in deoxyperidinin is due to a variety of intrinsic electronic properties, but the most important of these is a decrease in the inhomogeneous broadening in deoxyperidinin relative to peridinin. The EOM-CCSD calculations also suggest that there is a larger separation of the $2^1A_g^-$ from the $1^1B_u^+$ state in deoxyperidinin, which leads to greater resolution of the S_0 ($1^1A_g^-$) $\rightarrow$ S_1 ($2^1A_g^-$) transition despite the prediction of a lower oscillator strength. Moreover, the EOM-CCSD calculations support the experimental observation that deoxyperidinin does not form an ICT state, regardless of solvent polarity. The lowest-lying excited singlet state is calculated to be a pure covalent $2^1A_g^-$ state in all solvents, including acetonitrile (see Figure 10).

An additional theoretical goal is to explain the presence of the prominent low-energy transition in the TA spectra of deoxyperidinin that is observed along with the well-characterized, higher-energy S_1 ($2^1A_g^-$) $\rightarrow$ S_n ($n^1B_u^+$) transition (Figure 6). As mentioned above, the low-energy band is hardly affected by solvent polarity and has a similar line width, intensity, and dynamics as the higher-energy S_1 ($2^1A_g^-$) $\rightarrow$ S_n ($n^1B_u^+$) transition. This suggests that it also arises from an S_1 ($2^1A_g^-$) $\rightarrow$ $^1B_u^+$ transition. No such transition has ever been reported for a carotenoid, but computations based on MNDO-PSDCI theory reveal precisely this transition for deoxyperidinin (top panel in Figure 12). Note that the model reproduces the experimental ESA features shown in Figure 6 very well in that two transitions originating from S_1 ($2^1A_g^-$) having similar amplitudes are predicted to occur with >100 nm separation in the visible spectral region. Interestingly, this same quantum mechanical model also predicts low-energy features for peridinin (bottom panel in Figure 12). Up to this point, excited state absorption bands in this region for peridinin have been attributed to an ICT $\rightarrow$ S_n transition, especially in polar solvents.[26,55,64] However, a closer examination of the TA spectrum of peridinin recorded at room temperature in the nonpolar solvent, *n*-hexane, i.e., conditions under which the ICT $\rightarrow$ S_n band amplitude is likely to be kept to a minimum, reveals the presence of at least one structured band[26,55] that is, in fact, consistent with the present predictions of the MNDO-PSDCI theoretical model. These lower-energy features could be rendered smaller relative to the main S_1 ($2^1A_g^-$) $\rightarrow$ S_n ($n^1B_u^+$) transition in the experimental TA spectra of peridinin due to inhomogeneous broadening effects like those described above that affect the steady-state spectra. Most certainly, the features would be concealed completely by the intense ICT $\rightarrow$ S_n band that is formed in that spectral region when the molecule is dissolved in polar solvents.

CONCLUSIONS

By synthesizing an analogue of peridinin in which the π-electron conjugated carbonyl group in its lactone ring has been eliminated, deoxyperidinin has provided the means by which

DOI: 10.1021/acs.jpcb.6b00439
J. Phys. Chem. B 2016, 120, 2731−2744

the energy state complexion and spectroscopic properties of both peridinin and deoxyperidinin have become more apparent. In experiments carried out at 77 K, features in the steady-state absorption spectrum of deoxyperidinin were unambiguously assigned to the forbidden S_0 ($1^1A_g^-$) → S_1 ($2^1A_g^-$) transition. These features became evident due to a substantial reduction in both molecular conformational disorder and inhomogeneous broadening of the spectra of deoxyperidinin compared to peridinin. Ultrafast time-resolved transient fluorescence and absorption experiments examined the excited state spectra and dynamics of deoxyperidinin. The steady-state and time-resolved spectra were interpreted within the framework of quantum computations that revealed the key electronic mechanisms leading to the observation of the forbidden S_0 ($1^1A_g^-$) → S_1 ($2^1A_g^-$) transition in the absorption spectrum of deoxyperidinin. One of these mechanisms involves the increased separation between the positions of the S_0 ($1^1A_g^-$) → S_1 ($2^1A_g^-$) and S_0 ($1^1A_g^-$) → S_2 ($1^1B_u^+$) transitions. More importantly, the dominant contributing property is linked to the reduction of solvent-induced inhomogeneous broadening in the spectra of deoxyperidinin, which is associated with a significantly smaller change in dipole moment upon transition to the first two excited singlet states of deoxyperidinin relative to peridinin.

AUTHOR INFORMATION

Corresponding Author

*Phone: 860-486-2844. Fax: 860-486-6558. E-mail: harry.frank@uconn.edu.

Notes

The authors declare no competing financial interest.

ACKNOWLEDGMENTS

Work in the laboratory of H.A.F. was supported by grants from the National Science Foundation (MCB-1243565) and the University of Connecticut Research Foundation. Work in the laboratory of R.R.B. was supported by grants from the National Institutes of Health (GM-34548) and the Harold S. Schwenk Sr. Distinguished Chair in Chemistry. S.K. acknowledges support from the Grant-in-Aid for Scientific Research (C) (25410183 and 26410183) from the Japan Society of the Promotion of Science (JSPS). Ultrafast spectroscopy was jointly performed by D.M.N. and N.C.M.M. associated with the Ultrafast Laser Facility of the Photosynthetic Antenna Research Center, an Energy Frontier Research Center funded by the U.S. Department of Energy, Office of Science, Office of Basic Energy Sciences under Award Number DE-SC 0001035.

REFERENCES

(1) Tavan, P.; Schulten, K. Electronic Excitations in Finite and Infinite Polyenes. *Phys. Rev. B: Condens. Matter Mater. Phys.* **1987**, *36*, 4337−4358.

(2) Hudson, B.; Kohler, B. Linear Polyene Electronic Structure and Spectroscopy. *Annu. Rev. Phys. Chem.* **1974**, *25*, 437−460.

(3) Hudson, B. S.; Kohler, B. E. Polyene Spectroscopy: The Lowest Energy Excited Single State of Diphenyloctatetraene and Other Linear Polyenes. *J. Chem. Phys.* **1973**, *59*, 4984−5002.

(4) Hudson, B. S.; Kohler, B. E.; Schulten, K. Linear Polyene Electronic Structure and Potential Surfaces. In *Excited States*; Lim, E. D., Ed.; Academic Press: New York, 1982; Vol. *6*, pp 1−95.

(5) Schulten, K.; Karplus, M. On the Origin of a Low-Lying Forbidden Transition in Polyenes and Related Molecules. *Chem. Phys. Lett.* **1972**, *14*, 305−309.

(6) Tavan, P.; Schulten, K. The 2^1A_g - 1^1B_u Energy Gap in the Polyenes: An Extended Configuration Interaction Study. *J. Chem. Phys.* **1979**, *70*, 5407−5413.

(7) Britton, G. UV/Visible Spectroscopy. In *Carotenoids, Vol. 1b: Spectroscopy*; Britton, G., Liaaen-Jensen, S., Pfander, H., Eds.; Birkhäuser Verlag: Basel-Boston-Berlin, 1995; pp 13−62.

(8) Herzberg, G.; Teller, E. Fluctuation Structure of Electron Transfer in Multiatomic Molecules. *Z. Phys. Chem., Abt. B* **1933**, *21*, 410−446.

(9) Frank, H. A.; Desamero, R. Z. B.; Chynwat, V.; Gebhard, R.; van der Hoef, I.; Jansen, F. J.; Lugtenburg, J.; Gosztola, D.; Wasielewski, M. R. Spectroscopic Properties of Spheroidene Analogs Having Different Extents of Π-Electron Conjugation. *J. Phys. Chem. A* **1997**, *101*, 149−157.

(10) Frank, H. A.; Josue, J. S.; Bautista, J. A.; van der Hoef, I.; Jansen, F. J.; Lugtenburg, J.; Wiederrecht, G.; Christensen, R. L. Spectroscopic and Photochemical Properties of Open-Chain Carotenoids. *J. Phys. Chem. B* **2002**, *106*, 2083−2092.

(11) Andersson, P. O.; Bachilo, S. M.; Chen, R.-L.; Gillbro, T. Solvent and Temperature Effects on Dual Fluorescence in a Series of Carotenes. Energy Gap Dependence of the Internal Conversion Rate. *J. Phys. Chem.* **1995**, *99*, 16199−16209.

(12) Fujii, R.; Onaka, K.; Kuki, M.; Koyama, Y.; Watanabe, Y. The $2A_g^-$ Energies of All-*Trans*-Neurosporene and Spheroidene as Determined by Fluorescence Spectroscopy. *Chem. Phys. Lett.* **1998**, *288*, 847−853.

(13) Fujii, R.; Ishikawa, T.; Koyama, Y.; Taguchi, M.; Isobe, Y.; Nagae, H.; Watanabe, Y. Fluorescence Spectroscopy of All-*Trans*-Anhydrorhodovibrin and Spirilloxanthin: Detection of the $1B_u^-$ Fluorescence. *J. Phys. Chem. A* **2001**, *105*, 5348−5355.

(14) Onaka, K.; Fujii, R.; Nagae, H.; Kuki, M.; Koyama, Y.; Watanabe, Y. The State Energy and the Displacements of the Potential Minima of the $2A_g^-$ State in All-*Trans*-B-Carotene as Determined by Fluorescence Spectroscopy. *Chem. Phys. Lett.* **1999**, *315*, 75−81.

(15) Frank, H. A.; Bautista, J. A.; Josue, J.; Pendon, Z.; Hiller, R. G.; Sharples, F. P.; Gosztola, D.; Wasielewski, M. R. Effect of the Solvent Environment on the Spectroscopic Properties and Dynamics of the Lowest Excited States of Carotenoids. *J. Phys. Chem. B* **2000**, *104*, 4569−4577.

(16) Mimuro, M.; Nagashima, U.; Takaichi, S.; Nishimura, Y.; Yamazaka, I.; Katoh, T. Molecular Structure and Optical Properties of Cartenoids for the *in Vivo* Energy Transfer Function in Algal Photosynthetic Pigment System. *Biochim. Biophys. Acta, Bioenerg.* **1992**, *1098*, 271−274.

(17) Zhang, J.-P.; Fujii, R.; Qian, P.; Inaba, T.; Mizoguchi, T.; Koyama, Y.; Onaka, K.; Watanabe, Y. Mechanism of the Carotenoid-to-Bacteriochlorophyll Energy Transfer Via the S_1 State in the LH2 Complexes from Purple Bacteria. *J. Phys. Chem. B* **2000**, *104*, 3683−3691.

(18) Hsu, C. P.; Walla, P. J.; Head-Gordon, M.; Fleming, G. R. The Role of the S-1 State of Carotenoids in Photosynthetic Energy Transfer: The Light-Harvesting Complex II of Purple Bacteria. *J. Phys. Chem. B* **2001**, *105*, 11016−11025.

(19) Wang, P.; Nakamura, R.; Kanematsu, Y.; Koyama, Y.; Nagae, H.; Nishio, T.; Hashimoto, H.; Zhang, J. P. Low-Lying Singlet States of Carotenoids Having 8−13 Conjugated Double Bonds as Determined by Electronic Absorption Spectroscopy. *Chem. Phys. Lett.* **2005**, *410*, 108−114.

(20) Polívka, T.; Frank, H. A. Molecular Factors Controlling Photosynthetic Light Harvesting by Carotenoids. *Acc. Chem. Res.* **2010**, *43*, 1125−1134.

(21) Bautista, J. A.; Hiller, R. G.; Sharples, F. P.; Gosztola, D.; Wasielewski, M.; Frank, H. A. Singlet and Triplet Energy Transfer in the Peridinin-Chlorophyll *a*-Protein from *Amphidinium carterae*. *J. Phys. Chem. A* **1999**, *103*, 2267−2273.

(22) Zigmantas, D.; Hiller, R. G.; Sundström, V.; Polivka, T. Carotenoid to Chlorophyll Energy Transfer in the Peridinin Chlorophyll-*a* Protein Complex Involves an Intramolecular Charge Transfer State. *Proc. Natl. Acad. Sci. U. S. A.* **2002**, *99*, 16760−16765.

DOI: 10.1021/acs.jpcb.6b00439
J. Phys. Chem. B 2016, 120, 2731−2744

(23) Krueger, B. P.; Lampoura, S. S.; van Stokkum, I. H. M.; Papagiannakis, E.; Salverda, J. M.; Gradinaru, C. C.; Rutkauskas, D.; Hiller, R. G.; van Grondelle, R. Energy Transfer in the Peridinin Chlorophyll *a* Protein of *Amphidinium carterae* Studied by Polarized Transient Absorption and Target Analysis. *Biophys. J.* **2001**, *80*, 2843−2855.
(24) Shima, S.; Ilagan, R. P.; Gillespie, N.; Sommer, B. J.; Hiller, R. G.; Sharples, F. P.; Frank, H. A.; Birge, R. R. Two-Photon and Fluorescence Spectroscopy and the Effect of Environment on the Photochemical Properties of Peridinin in Solution and in the Peridinin-Chlorophyll-Protein from *Amphidinium carterae*. *J. Phys. Chem. A* **2003**, *107*, 8052−8066.
(25) Chatterjee, N.; Niedzwiedzki, D. M.; Aoki, K.; Kajikawa, T.; Katsumura, S.; Hashimoto, H.; Frank, H. A. Effect of Structural Modifications on the Spectroscopic Properties and Dynamics of the Excited States of Peridinin. *Arch. Biochem. Biophys.* **2009**, *483*, 146−155.
(26) Niedzwiedzki, D. M.; Chatterjee, N.; Enriquez, M. M.; Kajikawa, T.; Hasegawa, S.; Katsumura, S.; Frank, H. A. Spectroscopic Investigation of Peridinin Analogues Having Different Π-Electron Conjugated Chain Lengths: Exploring the Nature of the Intramolecular Charge Transfer State. *J. Phys. Chem. B* **2009**, *113*, 13604−13612.
(27) Niedzwiedzki, D. M.; Kajikawa, T.; Aoki, K.; Katsumura, S.; Frank, H. A. Excited State Energies and Dynamics of Peridinin Analogues and the Nature of the Intramolecular Charge Transfer (ICT) State in Carbonyl-Containing Carotenoids. *J. Phys. Chem. B* **2013**, *117*, 6874−6887.
(28) Fuciman, M.; Enriquez, M. M.; Kaligotla, S.; Niedzwiedzki, D. M.; Kajikawa, T.; Aoki, K.; Katsumura, S.; Frank, H. A. Singlet and Triplet State Spectra and Dynamics of Structurally Modified Peridinins. *J. Phys. Chem. B* **2011**, *115*, 4436−4445.
(29) Bautista, J. A.; Connors, R. E.; Raju, B. B.; Hiller, R. G.; Sharples, F. P.; Gosztola, D.; Wasielewski, M. R.; Frank, H. A. Excited State Properties of Peridinin: Observation of a Solvent Dependence of the Lowest Excited Singlet State Lifetime and Spectral Behavior Unique among Carotenoids. *J. Phys. Chem. B* **1999**, *103*, 8751−8758.
(30) Enriquez, M. M.; Hananoki, S.; Hasegawa, S.; Kajikawa, T.; Katsumura, S.; Wagner, N. L.; Birge, R. R.; Frank, H. A. Effect of Molecular Symmetry on the Spectra and Dynamics of the Intramolecular Charge Transfer (ICT) State of Peridinin. *J. Phys. Chem. B* **2012**, *116*, 10748−10756.
(31) Niedzwiedzki, D. M.; Jiang, J.; Lo, C. S.; Blankenship, R. E. Low-Temperature Spectroscopic Properties of the Peridinin−Chlorophyll *a*−Protein (PCP) Complex from the Coral Symbiotic Dinoflagellate *Symbiodinium*. *J. Phys. Chem. B* **2013**, *117*, 11091−11099.
(32) Martin, C. H.; Birge, R. R. Reparameterizing MNDO for Excited State Calculations Using *Ab Initio* Effective Hamiltonian Theory: Application to the 2,4-Pentadien-1-Iminium Cation. *J. Phys. Chem. A* **1998**, *102*, 852−860.
(33) Pendon, Z. D.; Sullivan, J. O.; van der Hoef, I.; Lugtenburg, J.; Cua, A.; Bocian, D. F.; Birge, R. R.; Frank, H. A. Stereoisomers of Carotenoids: Spectroscopic Properties of Locked and Unlocked cis-Isomers of Spheroidene. *Photosynth. Res.* **2005**, *86*, 5−24.
(34) Niedzwiedzki, D. M.; Sandberg, D. J.; Cong, H.; Sandberg, M. N.; Gibson, G. N.; Birge, R. R.; Frank, H. A. Ultrafast Time-Resolved Absorption Spectroscopy of Geometric Isomers of Carotenoids. *Chem. Phys.* **2009**, *357*, 4−16.
(35) Wagner, N. L.; Greco, J. A.; Enriquez, M. M.; Frank, H. A.; Birge, R. R. The Nature of the Intramolecular Charge Transfer (ICT) State in Peridinin. *Biophys. J.* **2013**, *104*, 1314−1325.
(36) Birge, R. R.; Schulten, K.; Karplus, M. Possible Influences of a Low-Lying 'Covalent' Excited State on the Absorption Spectrum and Photoisomerization of 11-cis Retinal. *Chem. Phys. Lett.* **1975**, *31*, 451−454.
(37) Stanton, J. F.; Bartlett, R. J. Equation Motion Coupled-Cluster Method: A Systematic Biorthogonal Approach to Molecular Excitation Energies, Transition Probabilities, and Excited State Properties. *J. Chem. Phys.* **1993**, *98*, 7029−7039.
(38) Koch, H.; Kobayashi, R.; Sánchez de Merás, A.; Jørgensen, P. Calculation of Size-Intensive Transition Moments from the Coupled Cluster Singles and Doubles Linear Response Function. *J. Chem. Phys.* **1994**, *100*, 4393−4400.
(39) Kállay, M.; Gauss, J. Calculation of Excited-State Properties Using General Coupled-Cluster and Configuration-Interaction Models. *J. Chem. Phys.* **2004**, *121*, 9257−9269.
(40) Krylov, A. I. Equation-of-Motion Coupled-Cluster Methods for Open-Shell and Electronically Excited Species: The Hitchhiker's Guide to Fock Space. *Annu. Rev. Phys. Chem.* **2008**, *59*, 433−462.
(41) Head-Gordon, M.; Pople, J. A.; Frisch, M. J. MP2 Energy Evaluation by Direct Methods. *Chem. Phys. Lett.* **1988**, *153*, 503−506.
(42) Nakatsuji, H. Cluster Expansion of the Wavefunction. Excited States. *Chem. Phys. Lett.* **1978**, *59*, 362−364.
(43) Nakatsuji, H.; Hirao, K. Cluster Expansion of the Wavefunction. Symmetry-Adapted-Cluster Expansion, Its Variational Determination, and Extension of Open-Shell Orbital Theory. *J. Chem. Phys.* **1978**, *68*, 2053−2065.
(44) Nakatsuji, H. Description of Two- and Many-Electron Processes by the SAC-CI Method. *Chem. Phys. Lett.* **1991**, *177*, 331−337.
(45) Nakajima, T.; Nakatsuji, H. Energy Gradient Method for the Ground, Excited, Ionized, and Electron-Attached States Calculated by the SAC (Symmetry-Adapted Cluster)/SAC-CI (Configuration Interaction) Method. *Chem. Phys.* **1999**, *242*, 177−193.
(46) Frisch, M. J.; Trucks, G. W.; Schlegel, H. B.; Scuseria, G. E.; Robb, M. A.; Cheeseman, J. R.; Scalmani, G.; Barone, V.; Mennucci, B.; Petersson, G. A.; et al.; Gaussian, Inc.: Wallingford, CT, 2009.
(47) Dunning, T. H., Jr.; Hay, P. J. Modern Theoretical Chemistry. In *Modern Theoretical Chemistry*; Schaefer, H. F., Ed.; Plenum: New York, 1976; Vol. 3, pp 1−28.
(48) Birge, R. R.; Bocian, D. F.; Hubbard, L. M. Origins of Inhomogeneous Broadening in the Vibronic Spectra of Visual Chromophores and Visual Pigments. *J. Am. Chem. Soc.* **1982**, *104*, 1196−1207.
(49) Niedzwiedzki, D.; Koscielecki, J. F.; Cong, H.; Sullivan, J. O.; Gibson, G. N.; Birge, R. R.; Frank, H. A. Ultrafast Dynamics and Excited State Spectra of Open-Chain Carotenoids at Room and Low Temperatures. *J. Phys. Chem. B* **2007**, *111*, 5984−5998.
(50) Niedzwiedzki, D. M.; Enriquez, M. M.; LaFountain, A. M.; Frank, H. A. Ultrafast Time-Resolved Absorption Spectroscopy of Geometric Isomers of Xanthophylls. *Chem. Phys.* **2010**, *373*, 80−89.
(51) Krawczyk, S.; Olszowka, D. Spectral Broadening and Its Effect in Stark Spectra of Carotenoids. *Chem. Phys.* **2001**, *265*, 335−347.
(52) van Stokkum, I. H. M.; Larsen, D. S.; van Grondelle, R. Global and Target Analysis of Time-Resolved Spectra. *Biochim. Biophys. Acta, Bioenerg.* **2004**, *1657*, 82−104.
(53) Polívka, T.; Sundström, V. Ultrafast Dynamics of Carotenoids Excited States - from Solution to Natural and Artificial Systems. *Chem. Rev.* **2004**, *104*, 2021−2071.
(54) Papagiannakis, E.; Vengris, M.; Larsen, D. S.; van Stokkum, I. H. M.; Hiller, R. G.; van Grondelle, R. Use of Ultrafast Dispersed Pump-Dump-Probe and Pump-Repump-Probe Spectroscopies to Explore the Light-Induced Dynamics of Peridinin in Solution. *J. Phys. Chem. B* **2006**, *110*, 512−521.
(55) Zigmantas, D.; Hiller, R. G.; Yartsev, A.; Sundström, V.; Polivka, T. Dynamics of Excited States of the Carotenoid Peridinin in Polar Solvents: Dependence on Excitation Wavelength, Viscosity, and Temperature. *J. Phys. Chem. B* **2003**, *107*, 5339−5348.
(56) Zigmantas, D.; Hiller, R. G.; Sharples, F. P.; Frank, H. A.; Sundström, V.; Polivka, T. Effect of a Conjugated Carbonyl Group on the Photophysical Properties of Carotenoids. *Phys. Chem. Chem. Phys.* **2004**, *6*, 3009−3016.
(57) Yoshizawa, M.; Kosumi, D.; Komukai, M.; Hashimoto, H. Ultrafast Optical Responses of Three-Level Systems in Beta-Carotene: Resonance to a High-Lying N(1) a(G)(−) Excited State. *Laser Phys.* **2006**, *16*, 325−330.
(58) Polívka, T.; Herek, J. L.; Zigmantas, D.; Akerlund, H. E.; Sundström, V. Direct Observation of the (Forbidden) S_1 State in Carotenoids. *Proc. Natl. Acad. Sci. U. S. A.* **1999**, *96*, 4914−4917.

DOI: 10.1021/acs.jpcb.6b00439
J. Phys. Chem. B 2016, 120, 2731−2744

(59) Polívka, T.; Zigmantas, D.; Herek, J. L.; He, Z.; Pascher, T.; Pullerits, T.; Cogdell, R. J.; Frank, H. A.; Sundström, V. The Carotenoid S_1 State in LH2 Complexes from Purple Bacteria *Rhodobacter spheroides* and *Rhodopseudomonas acidophila*: S1 Energies, Dynamics, and Carotenoid Radical Formation. *J. Phys. Chem. B* **2002**, *106*, 11016−11025.
(60) Niedzwiedzki, D. M.; Collins, A. M.; LaFountain, A. M.; Enriquez, M. M.; Frank, H. A.; Blankenship, R. E. Spectroscopic Studies of Carotenoid-to-Bacteriochlorophyll Energy Transfer in LHRC Photosynthetic Complex from *Roseiflexus castenholzii*. *J. Phys. Chem. B* **2010**, *114*, 8723−8734.
(61) Hashimoto, H.; Koyama, Y.; Hirata, Y.; Mataga, N. S_1 and T_1 Species of B-Carotene Generated by Direct Photoexcitation from the All-*trans*, 9-*cis*, 13-*cis*, and 15-*cis* Isomers as Revealed by Picosecond Transient Absorption and Transient Raman Spectroscopies. *J. Phys. Chem.* **1991**, *95*, 3072−3076.
(62) Enriquez, M. M.; Fuciman, M.; LaFountain, A. M.; Wagner, N. L.; Birge, R. R.; Frank, H. A. The Intramolecular Charge Transfer State in Carbonyl-Containing Polyenes and Carotenoids. *J. Phys. Chem. B* **2010**, *114*, 12416−12426.
(63) Greco, J. A.; Shima, S.; Wagner, N. L.; McCarthy, J. R.; Atticks, K.; Bruckner, C.; Birge, R. R. Two-Photon Spectroscopy of the Q-Bands of Meso-Tetraphenyl- Porphyrin and -Chlorin Framework Derivatives. *J. Phys. Chem. C* **2015**, *119*, 3711−3724.
(64) Zigmantas, D.; Polivka, T.; Hiller, R. G.; Yartsev, A.; Sundström, V. Spectroscopic and Dynamic Properties of the Peridinin Lowest Singlet Excited States. *J. Phys. Chem. A* **2001**, *105*, 10296−10306.

DOI: 10.1021/acs.jpcb.6b00439
J. Phys. Chem. B 2016, 120, 2731−2744